ORIGINAL PAPER

Structural, Optical and Antibacterial Properties of Green Synthesized Silver Nanoparticles (AgNPs) Using *Justicia adhatoda* L. Leaf Extract

N. Thirumagal[1] · A. Pricilla Jeyakumari[1]

Abstract

Recently, AgNPs were used as a potential candidate for the applications of the human contacting areas such as cosmetics, food and medicine. Based on the above facts, in the present investigation, synthesis of silver nanoparticle was done using *Justicia adhatoda leaf* extract. The AgNPs were synthesized by bioreduction method of silver nitrate at different concentrations of *J. adhatoda l*eaf extract (10, 20, 30, 40 ml). It was characterized by a powder X-ray diffraction technique, SEM (Scanning Electron Microscope) with EDAX and FTIR (Fourier Transform Infrared Spectroscopy). It exhibited face centered cubic structure and the particle size was found to be 30 nm and the lattice strain (W–H plot) was 0.0079. The functional groups present in the compound were confirmed by the FTIR spectrum (424 cm^{-1} and 402 cm^{-1}). In this work spherical morphology of the particles at different concentrations was identified by TEM (particles size 16–21 nm) and SEM images. The optical energy band gap was found to be 2.9 eV from the UV–Vis spectrum. Zeta potential of AgNPs was determined as − 17.2 nm. The antibacterial activity of the synthesized AgNPs was tested using both gram positive bacteria (*Staphylococcus aureus*) and gram negative bacteria (*Escherichia coli*) and concluded that it may be a harmful nanomedicine for respiratory track ailments.

Keywords AgNPs · *Justicia adhatoda* · TEM · SEM · Antibacterial activity

Introduction

Nanoparticles are the building blocks of nanotechnology. Noble metals like Ag, Pt, Au, and Pd are applied in the field of nanomedicine and biotechnology [1]. In chemical and physical processes, a large number of solvents are required for obtaining pure and well-defined nanoparticles. They create various problems in the ecosystem and the environment [2].

There are several ways to reduce $AgNo_3$ into Ag^+. For example γ rays [3], UV irradiation [4], an electrochemical method [5], a reducing agent such as sodium borohydride [6–8] and polyethylene glycerol [9]. Surface effects and quantum effects are two factors that differentiate nanomaterials from the bulk. The optical and physical properties are unique in nanosilver, but not in bulk silver. Metallic silver is a malleable and ductile transition metal. It has the highest electrical and thermal conductivity, low contact resistance, and high optical reflectivity.

In nanomaterials, oxygen deficiency and large surface area are the two important parameters used in many scientific and industrial applications like catalysis, electronics and antibacterial activity. Antibacterial activities from silver are obtained due to the formation of reactive oxygen species (ROS) and disruption of membrane functionality. Formation of ROS causes oxidative stress which leads to cellular damage. The interaction between the release of ions in nano-sized silver results in the disruption of the membrane functionality. Silver nanoparticles can interact with the cell surface of various bacteria and form free radicals by AgNPs. When it interacts with the bacteria cells, it takes silver ions which inhibit several functions in the cells. It produced respiratory enzymes by silver ions and attacks the cell. The major components presented in DNA are sulfur and phosphorus nanoparticles which act on this and destroy the DNA that leads to cell death.

✉ A. Pricilla Jeyakumari
   pricilla1510@gmail.com

[1] Department of Physics, Thiruvalluvar Government Arts College, Rasipuram, Tamil Nadu, India

In recent years, plant meditating synthesis has become simple and eco-friendly. Most of the plant parts like leaves, seeds, flowers, and other parts are used as reducing and stabilizing agents in the synthesis of nanoparticles, but only few reports has been mentioned: *Azadirachta indica* [10], *Aloe vera* [11], *Banana Peel* [12], *Lanthana camera fruit* [13], *Tansi fruit* [14], *Ocimum basillicum* [15], *Carica papaya* [16], *Emblica officinalis* [17], *Morinda tinctoria* [18], *Catharanthus roseus* [19], *Coffee and Tea* [20], *Ziziphus jujuba* [21] etc. The *Justicia adhatoda* leaf contains phytochemicals such as alkaloids, tannins, saponins, phenolics and flavonoids. Adhatoda is a commonly available plant. It does not include the addition of any external stabilization. The synthesis cost-effective over chemical and physical methods and environment-friendly. Since there is no need to use high pressure, energy, temperature, toxic chemical and technology is very simple.

Motivated by the above facts, in the present study, silver nanoparticles (AgNPs) are synthesized from *J. adhatoda* leaf extract. Then it is characterized by X-ray diffraction FTIR analysis. The optical properties were determined from the UV–Vis spectrum, photoluminescence, Dynamic Light Scattering, Zeta potential, Scanning electron microscope and Energy-dispersive X-ray spectroscopy, Transmission electron microscopy was taken to confirm the morphology, shape and size of the particle. The antibacterial evaluation also carried out and reported that *J. adhatoda* is biologically important nanomedicine for respiratory system activity.

Experimental

Materials and Method

Chemical and Plant Material Collected

Silver nitrate (AgNO3) was purchased from Mercury Scientific, Salem District. The fresh *J. adhatoda* leaves were collected from our college botanical garden, Rasipuram, Namakkal district, Tamilnadu, India. Identification was done by Dept. of Botany, St. Joseph's college, Tiruchirappalli-02, Tamilnadu, India. Voucher specimen number-2798 as shown in Fig. 1. Double distilled water was used for preparing aqueous solutions all over the experiments.

Preparation of Leaf Extracts

The leaves of *J. adhatoda* were collected from the garden and washed several times in tap water and dried up for 4 days. Then the leaves were crushed into a fine powder then 10 g powder was added to 100 ml of doubled distilled water in a beaker and it was covered with aluminum foil


Fig. 1 *Justicia adhatoda* plant

and then the solution was heated in the water bath at 60 °C for 30 min [22]. The extract was filtered using Whatman No. 1 paper and used for synthesis.

Synthesis of AgNPs

10 ml of leaf extract solution was added to 90 ml of silver nitrate (AgNO$_3$) solution. The mixture was kept at a water bath for 45 min. After 45 min the pale yellow color of the solution has been changed into brown [23]. This indicates the formation of silver nanoparticles due to the excitation of surface plasma resonance in metal nanoparticles.

Characterization Methods

The purified silver nanoparticles were frozen, and dried to evaluate their crystalline structure and to determine crystallite size of the nanoparticles using diffractometer (Bruker D8 Advance, Germany) equipped with CuKα (λ = 1.5418 Å) X-ray radiation source, in the 2θ range from 20 to 80. The crystallite sizes of these silver nanoparticles were calculated by using the Debye–Scherrer equation. FT-IR analysis was carried out by JASCO 460 PLUS FT-IR spectrometer in the range of 4000–400 cm^{-1}. The synthesized AgNPs sample was dried and grinded with KBr pellets and analyzed. The various modes of vibrations were identified to determine the different functional groups present in AgNPs. The particle morphology, shape and size of synthesized AgNPs were analyzed by scanning electron microscope (SEM) JEOL 6360TESCAN 10 kV machine. In this experiment, the thin film of the sample was deposited on the carbon-coated copper grid. EDAX was carried out to confirm the elements present in the biosynthesized silver nanoparticles using EDX JEOL 6360TESCAN instrument. The surface morphology shape and size of the synthesized AgNPs were measured by TEM (TenaiSpiritnG2) with 120 kV accelerating voltage and LaB$_6$ source. The size distribution of bioreduced silver nanoparticles was measured using DLS (Zetasizer Nano ZS ZEN3600, Malvern, UK). The mean size of particles inside

Fig. 2 The XRD pattern of synthesized AgNPs
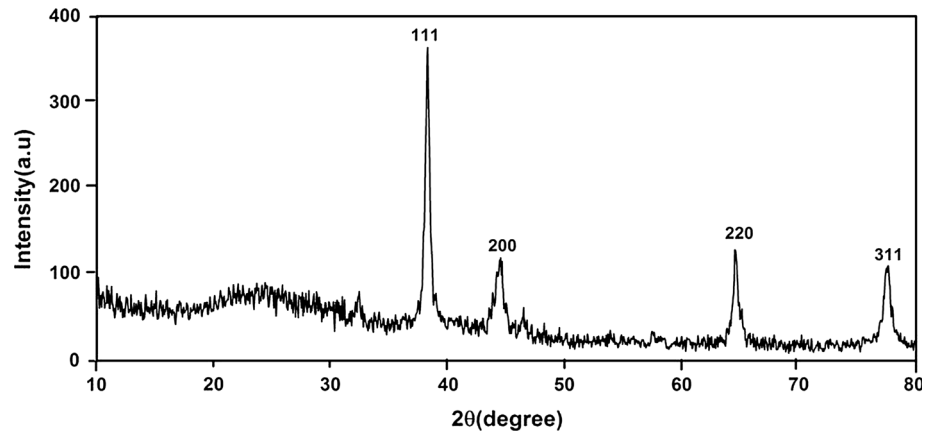
Fig. 3 The W–H plot of AgNPs
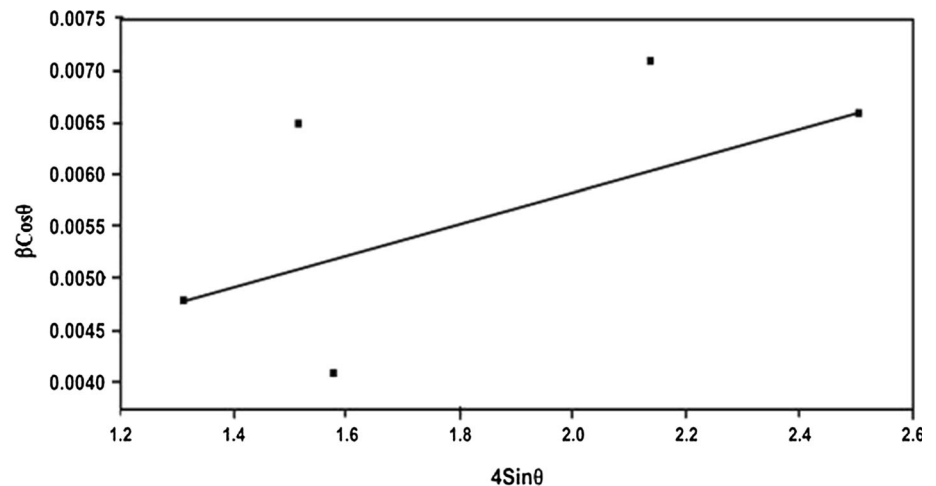
Table 1 Structural properties of FCC silver nanoparticles

| $2\theta^o$	d-spacing (Å)	Crystalline size D (nm)	Dislocation density ($\times 10^{14}$ lines/m^2)	Number of unit cells ($\times 10^6$)	Morphology index (MI)	Relative percentage error (RPE)
38.278	2.766	43.193	5.3619	4.7908	0.8856	0.7
44.493	2.036	25.806	1.5016	2.8793	0.3103	0.1
64.578	1.443	35.854	7.7790	2.886	0.9348	0.4
77.528	1.231	30.032	11.088	2.7525	0.3913	0.2

the sample is obtained with this measurement along with the correlation between the number of particles of a particular size vs. the size of the AgNPs. Zeta-potential measurements were done with a Zetasizer Nano ZS (Malvern Instruments) in a disposable cell at 25 °C using Zetasizer 7.01 software. Zeta potential measurements were used to study the stability of AgNPs. Biosynthesized AgNPs was analyzed by using UV–Vis spectrum (Lambda 35). The fluorescence spectrum was measured on a Perkin Elmer Lambda 45 in the range of 200–900 nm. The antibacterial activity of synthesized AgNPs has experimented with *Staphylococcus aureus* and *Escherichia coli* bacterium by agar disc diffusion technique.

Antibacterial Assay

The antibacterial activity of silver nanoparticles was tested against both the gram positive and gram negative bacteria. Clinical isolates of *S. aureus*, *E. coli* were sub-cultured in nutrient broth for 24 h at 37 °C. This study was carried out in agar by well diffusion method. AgNPs was mixed with Milli-Q water to make 50 µg, 100 µg, 150 µg concentration of AgNPs, silver nitrate, leaf extract, for positive

Fig. 4 The FTIR spectra of *Justicia adhatoda* leaf extract and synthesized AgNPs
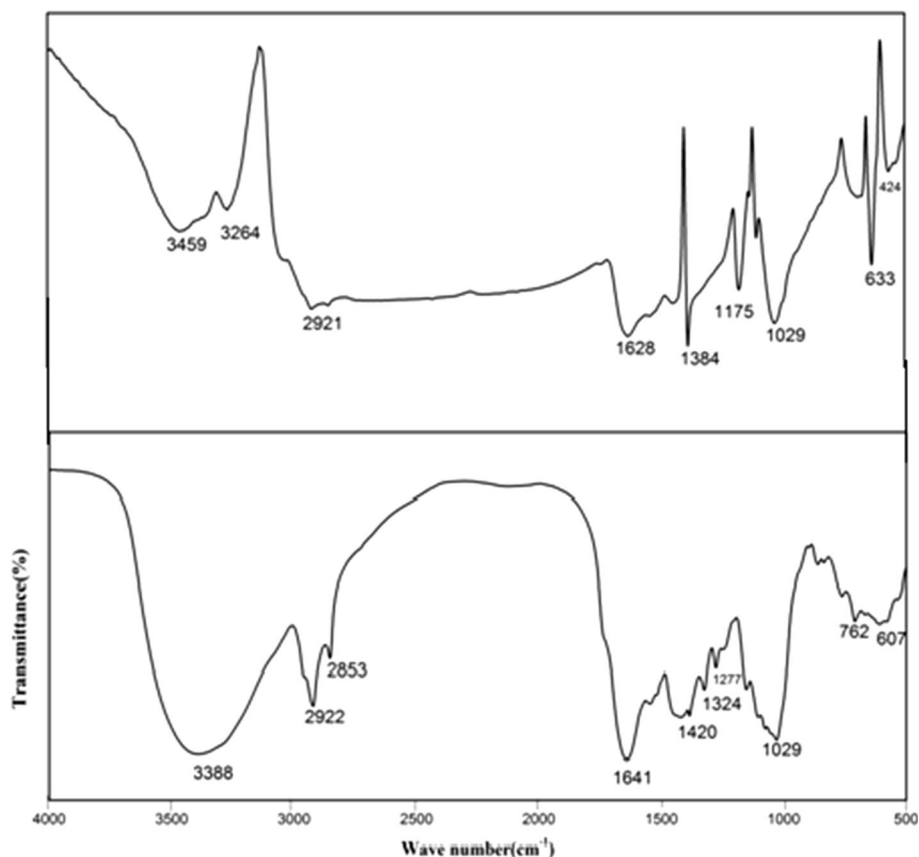
control Neomycin standard antibiotic (30 μg/ml), negative control Milli-Q water was used [24]. After 24 h of incubation at 37 °C. The Replicates were maintained throughout the experiments, then the zone of inhibition was measured.

Statistical Analysis

Each value is the mean of three replications each (n = 3). Statistically, the means of the three experiments were not significantly different (P < 0.05). Means in the same column with different letters are significantly different at (P < 0.05) in accordance with Fisher's least significant difference test. The statistical result shows that the synthesized silver nanoparticles are the potential candidate for enhancing the antibacterial property.

Results and Discussion

Structural and Morphology Study

X-ray diffraction pattern of synthesized powder AgNPs from *J. adhatoda* leaf extract was given in Fig. 2. It shows four high intensity peaks at 38.27°, 44.49°, 64.57°, 77.52° which

was corresponding to the diffraction signals arises from the planes (111) (200), (220) and (311) of the face centered cubic crystal of AgNPs (JCPDS file—04-0783) and the lattice parameter a = 4.717 Å. The average crystal size was calculated from XRD data using Scherrer's formula

$$D = k\lambda/\beta \cos\theta \qquad (1)$$

where D—crystallite size, λ—wavelength of the X-ray, θ—angle of diffraction and β—full width at half maximum (FWHM) are equated. The average crystallite size (D) of face centered cubic silver nanoparticles is 30 nm. Williamson–Hall method (Fig. 3) was used to find the lattice strain using the modified Scherrer equation [25].

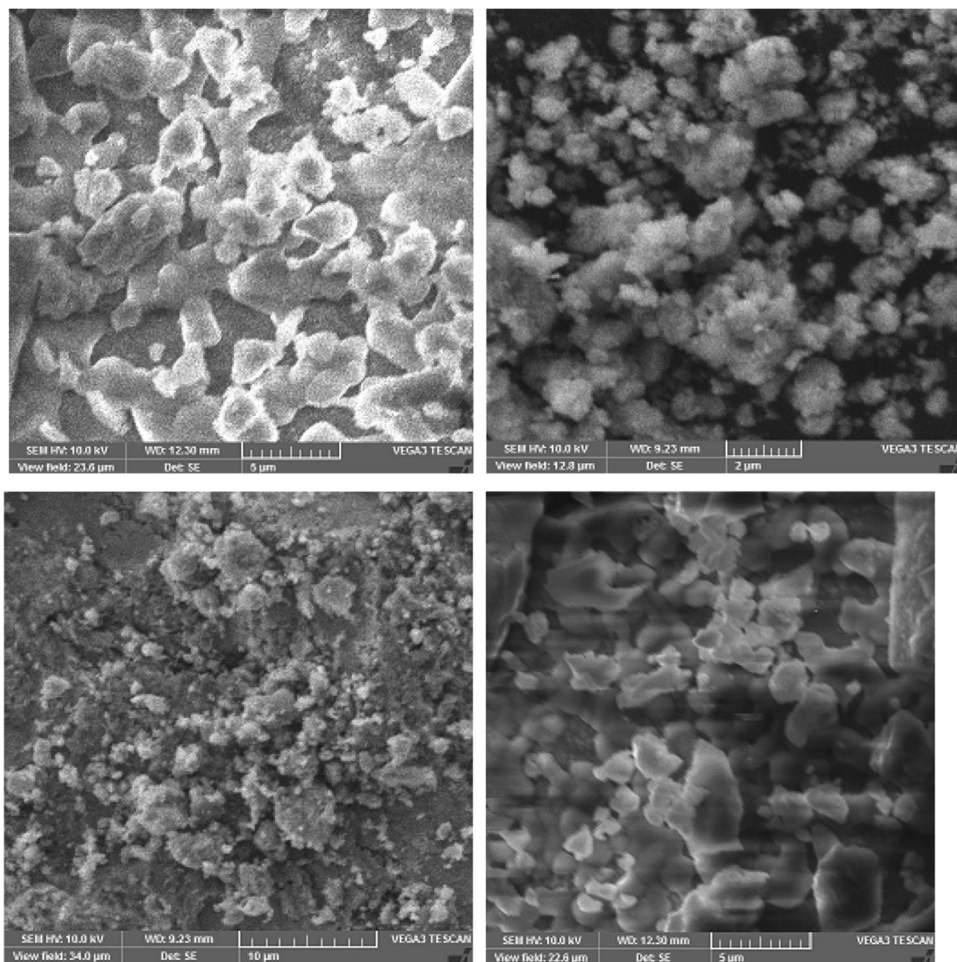$$\beta \cos\theta = (k\lambda/D) + (4\varepsilon \sin\theta) \qquad (2)$$

W–H plot of βcosθ Vs 4εsinθ shows the information about microstrain. Whereas the plot shows it has a non zero slope. The calculated value of microstrain for the prepared face centered cubic silver nanoparticles is 0.0079.

Dislocation Density (δ)

The dislocation density (δ) is calculated using the above equation.

$$\delta = 1/D^2 \qquad (3)$$

Fig. 5 The SEM images of synthesized AgNPs

The number of unit cells (n) is estimated from

$$n = (4/3)(D/2)^3(1/V) \qquad (4)$$

where V is the volume of the unit cell.

Morphology Index

The Morphology Index (MI) is calculated from the FWHM of XRD. MI is obtained using the equation below [26].

$$MI = FWHM_h/FWHM_h + FWHM_p \qquad (5)$$

where $FWHM_h$ is the highest FWHM value obtained from peaks, $FWHM_p$ is a value of particular peaks of FWHM. The calculated MI values are shown in Table 1.

Relative Percentage

The Relative Percentage Error (RPE) [26] is calculated by

$$RPE = (|Z_H - Z|/Z) \times 100 \qquad (6)$$

where Z_H is the experimental d-values in the XRD pattern and Z is the standard d-values in JCPDS data. The calculated RPE values are presented in Table 1.

FTIR Analysis

The functional group was confirmed by FTIR spectra (Fig. 4). The vibration modes at 3459–3264 cm^{-1} assigned for O–H stretching, the vibration of alcohol and phenol groups 2921 and 2922 cm^{-1} indicates that the stretching mode of C-H aliphatic. The peaks at 1641, 1628, and 2853 cm^{-1} are assigned to NH_3 asymmetric bending and CH_2 asymmetric stretching vibration. The peak at 1420 is assigned to C=C stretching mode in aromatic compounds. The peaks at 1324 and 1384 cm^{-1} are due to the stretching vibrations of the carboxyl group. The peaks at 1277 and 1029 cm^{-1} are due to COO^- and C–O stretching. Stretching bands at 762 and 607 cm^{-1} are disappeared in AgNPs. From the FTIR results, it is inferred that some of

Fig. 6 a–d SEM images of AgNPs show spherical morphology with different concentration of *Justicia adhatoda* extract **a** 10 ml, **b** 20 ml, **c** 30 ml, **d** 40 ml
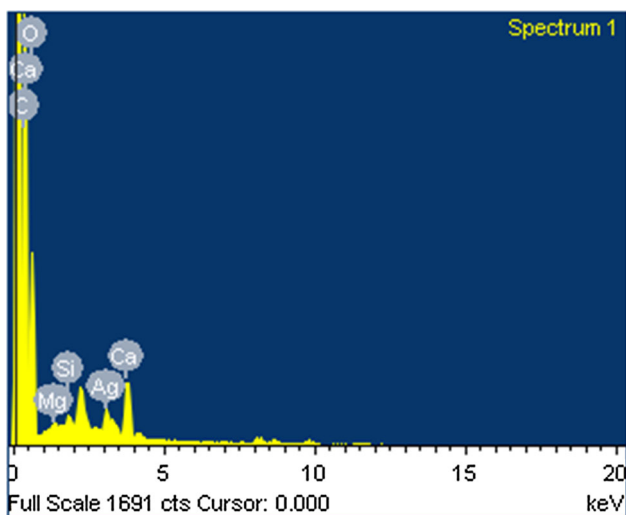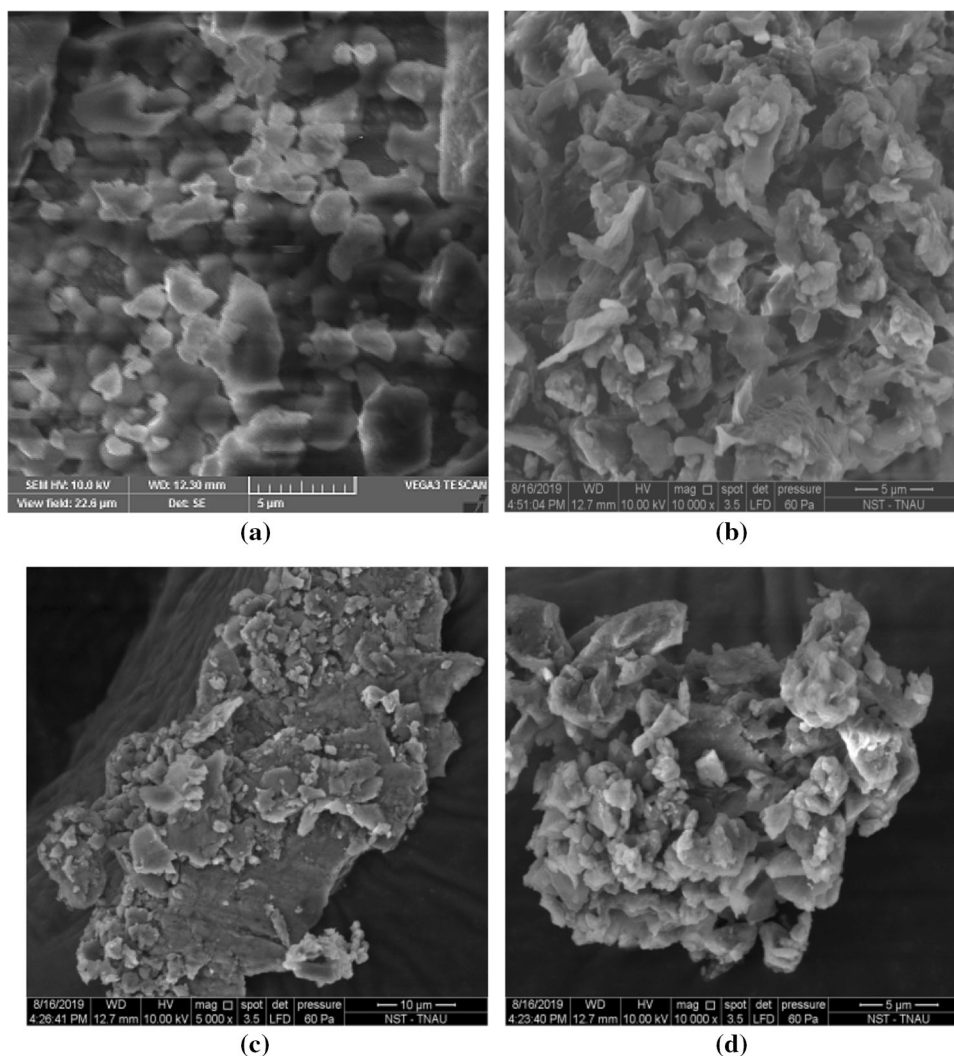
(a)

(b)

(c)

(d)

Fig. 7 The EDAX analysis of synthesized AgNPs

the bio-organics from broth *J. adhatoda* formed a strong capping on the nanoparticles. Formation of Ag^+ ion is at 633 and 424 cm^{-1} (Fig. 4) [27–29].

Morphological Analysis

The SEM images of the synthesized AgNPs in Fig. 5 showed the morphology of the prepared AgNPs is spherical due to the agglomerates of the particle distribution. SEM images are shown at different magnifications in Fig. 5 (10 μm, 5 μm, and 2 μm). The AgNPs are uniformly distributed with the size below 100 nm. These results are highly agreed with many earlier reports where biosynthesized AgNPs using different plant parts [30, 31]. Figure 6a–d shows the SEM images of different concentration 10, 20, 30, 40 ml of AgNPs. From the above observation, there is no appreciable change occurs in the morphology of the nanoparticles. It is clearly shows that the particles are spherical due to the agglomeration. Further, it is observed

Fig. 8 a–d TEM images of AgNPs show spherical morphology with different concentration of *Justicia adhatoda* leaf extract **a** 10 ml, **b** 20 ml, **c** 30 ml, **d** 40 ml
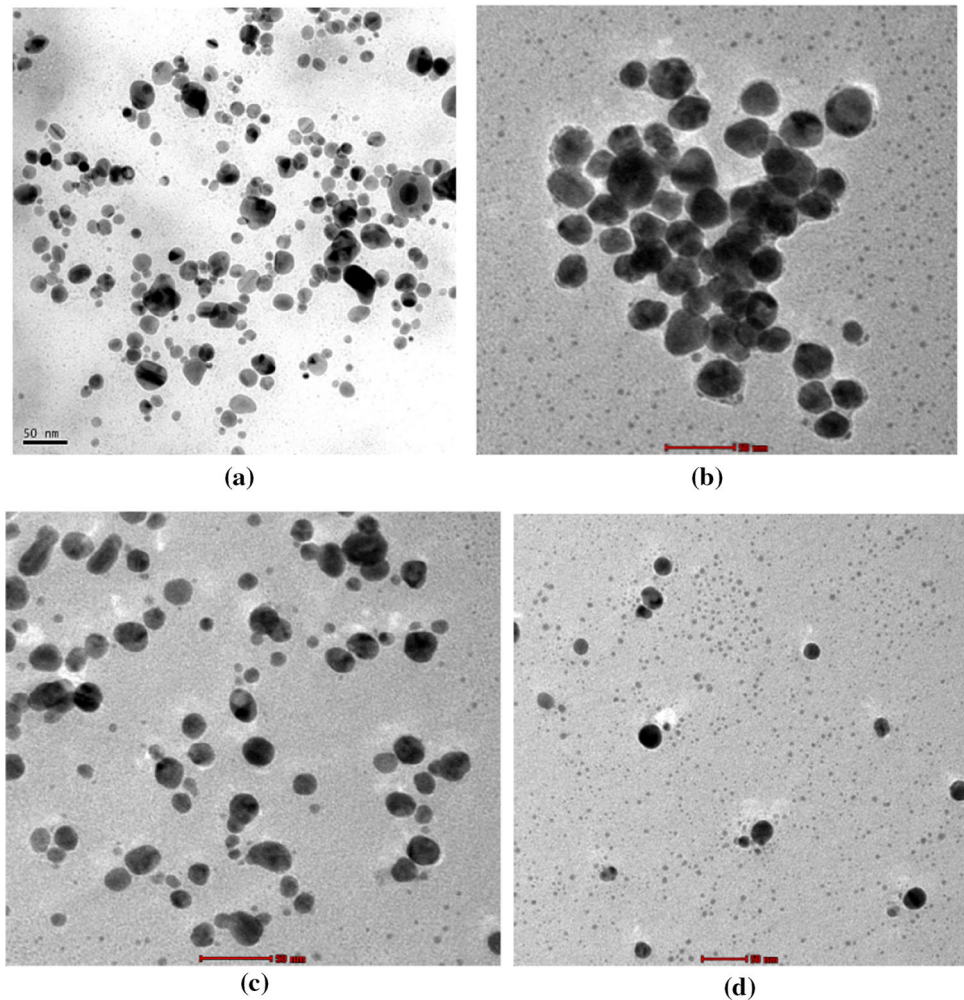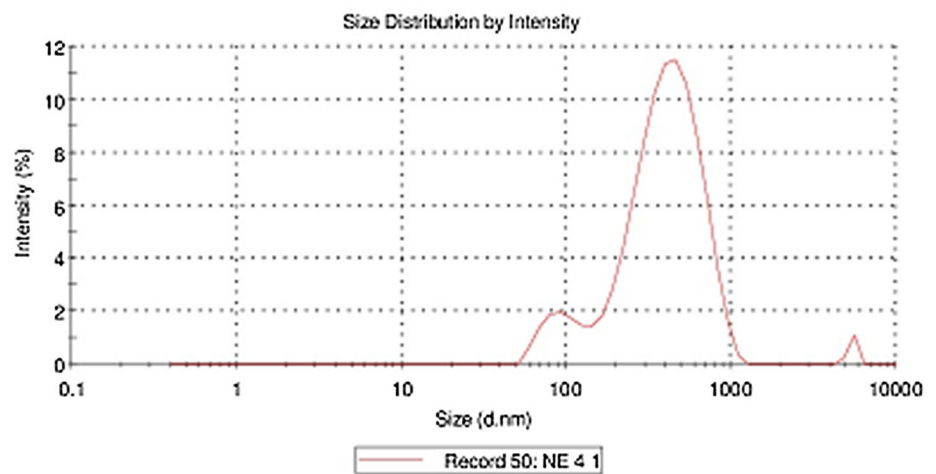

(a)

(b)

(c)

(d)

Fig. 9 The DLS pattern of synthesized AgNPs using *Justicia adhatoda* leaf extract

that microstructure is independent of the concentration of *J. adhatoda* leaf extract. The EDAX spectrum (Fig. 7) shows that the various elements presented in the prepared sample. TEM images of different concentrations 10, 20, 30, 40 ml of AgNPs are shown in Fig. 8a–d clearly shows that the silver nanoparticles are spherical and the size is found to be in the range of 16–21 nm.

Fig. 10 The Zeta potential stabilization pattern analysis of synthesized AgNPs using *Justicia adhatoda* leaf extract
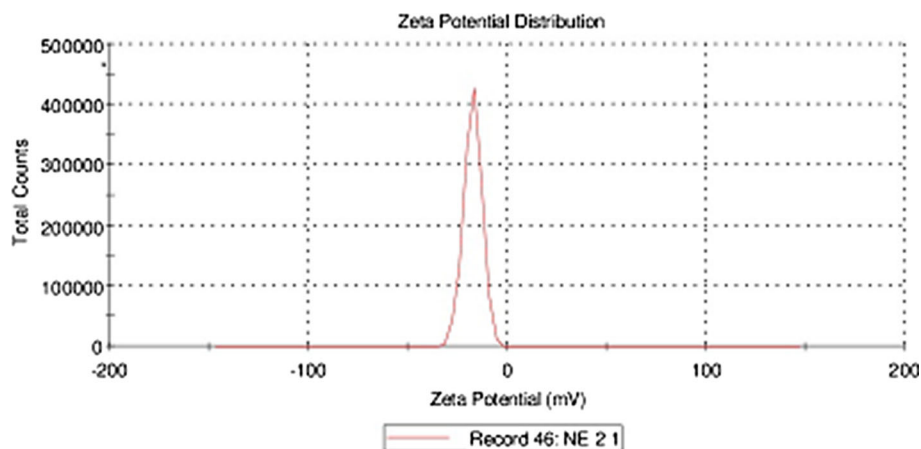
Dynamic Light Scattering (DLS) analysis

The average particle size of AgNPs is found to be 97 nm. The polydispersity index (PDI) of the AgNPs is determined by DLS, the intensity is 10.4%, and the width is 25.25 (d.nm). The PDI of AgNPs is 0.398 as shown in Fig. 9.

Zeta Potential Determination

The zeta potential of synthesized AgNPs was relatively stable. It was confirmed by the potential peak at − 17.2 mV and zeta deviation at 4.61 mV (Fig. 10) was determined from DLS. The results are compared with Gurunathan et al. [32]. The reported negative zeta potential values were due to the absorption of OH$^-$ ions in it. An OH$^-$ ion helps in preventing the aggregation and reducing the smaller size of AgNPs. It has also reported that greater potential has greater stability in the colloidal state [33].

Linear Optical Studies

The UV–Vis absorption spectrum of AgNPs was carried out by a UV–Vis spectrophotometer. The absorption peak at 417 nm of silver nanoparticles is shown in Fig. 11. Using the below equation, the optical bandgap is calculated.

$$\alpha h\nu = A\left(h\nu - E_g\right)^n \tag{7}$$

where α is the absorption coefficient, $h\nu$ is the photon energy, E_g is the optical band gap and A is constant. The parameter $n = 2$ is for direct allowed electron transition and $n = \frac{1}{2}$ for an indirect transition. The between $\alpha h\nu^2$ Vs $h\nu$ is shown in Fig. 12. From which the optical energy bandgap is estimated as 2.9 eV.

Fluorescence Studies

The fluorescence spectrum of silver nanoparticles was recorded in the range of 200–900 nm and the excitation
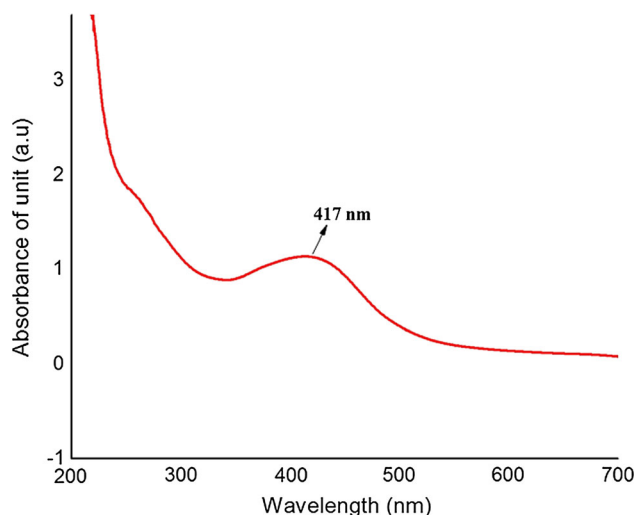

Fig. 11 The UV–Vis spectrum of AgNPs

wavelength is at 400 nm (Fig. 13). The spectrum shows that the two emission peaks at the wavelengths about 367 and 577 nm. The high-intensity peak was observed at 367 nm which indicates the blue emission region and 577 nm indicates the green emission region. Emission peaks lie in the visible region, which makes the material might be suitable for optoelectronic device fabrications [34].

Antibacterial Activity

The antibacterial activity was performed against the gram +ve bacteria *S. aureus* and gram −ve bacteria *E. coli*. The concentration of AgNPs is varied from 50 to 150 μg/ml as shown in Fig. 14. The most significant effect of AgNPs is found for the concentration of 150 μg/ml per disc. *E. coli* produces a better inhibition zone of gram negative bacteria while compared to *S. aureus* gram positive bacteria. The zone of inhibition of human pathogens is presented in
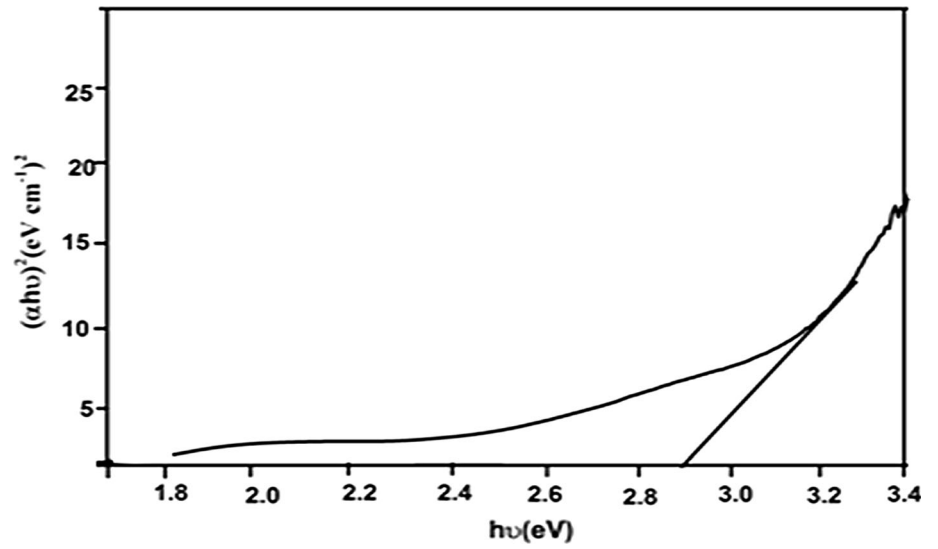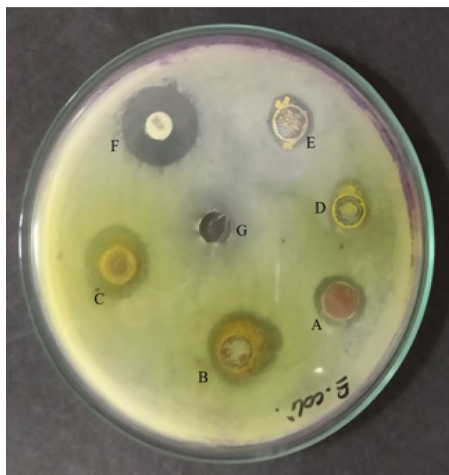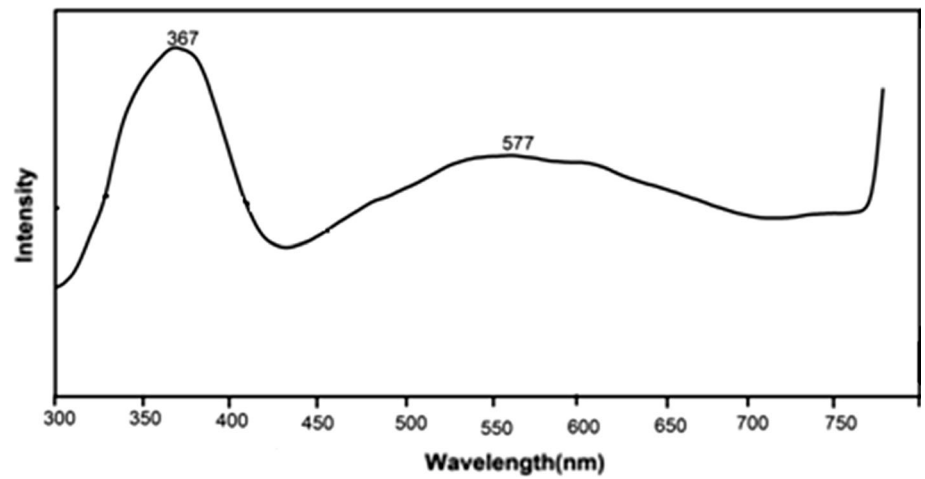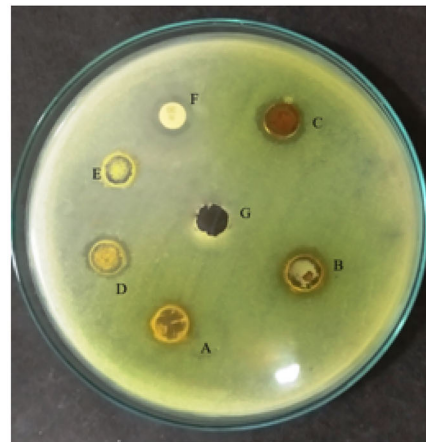
Fig. 12 The optical energy bandgap of AgNPs

Fig. 13 Fluorescence spectrum of synthesized AgNPs

Fig. 14 Plate photos of AgNPs using *Justicia adhatoda* leaf extract

Table 2 Antibacterial activity of AgNPs using *Justicia adhatoda* leaf extract concentration (50, 100, 150 µg/ml)

Tested bacteria	Zone of inhibition (mm)
Staphylococcus aureus	
A	7[c]
B	9[a]
C	9[a]
D	8[b]
E	7[c]
F	8[b]
G	0[d]
Escherichia coli	
A	13[d]
B	16[c]
C	17[b]
D	9[f]
E	10[e]
F	19[a]
G	0[g]

Antibiotic reference drug (F): neomycin

Each value is the mean of three replications each (n = 3). Statistically, the means of the three experiments were not significantly different (P < 0.05). Means in the same column with different letters (a–g) are significantly different at (P < 0.05) in accordance with Fisher's least significant difference test

Table 2. The observed antibacterial activity could be a binding of AgNPs to the cell wall. The cell membranes composed of the microorganism may cause damage to the respiration function of the cell [35, 36]. When metal ions Ag^+ is released by synthesized AgNPs using *J. adhatoda* leaf extract, it comes in contact with cell membranes of the microbes. The cell membranes with a negative charge and Ag^+ positive charge mutually attract penetrates the cell which causes the electrostatic attraction between bactericidal cell surface, which leads to the death of the microbes [37]. The detail antibacterial study shows that there are some biomedical and commercial applications for the synthesized AgNPs from *J. adhatoda*.

Conclusion

The Face centered cubic formation structure of AgNPs is confirmed by XRD, and the size of AgNPs was found to be 30 nm. SEM and TEM image showed a spherical shape of the AgNPs and the presence of Ag^+ ions was confirmed by EDAX analysis. The FTIR exhibited the stretching vibration mode of silver ions. The optical bandgap energy of AgNPs is 2.9 eV from the UV–Vis absorption spectrum. It shows that it may be the potential candidate for optoelectronic applications. They are polydispersed, and their spherical slopes were due to the agglomerates of the particle distribution. A maximum zone of inhibition was found for *E. coli* (17 nm) which exhibited the good antibacterial activity of the synthesized AgNPs. One of its high potential activities may be used in the preparation of cough syrup and nanomedicine for respiratory alignment.

References

1. R. Mata, J. R. Nakkala, and S. R. Sadras (2015). *Colloids Surf. B Biointerfaces.* **128**, 276–286.
2. P. Velmurugan, M. Cho, S.-S. Lim, S.-K. Seo, H. Myung, K.-S. Bang, S. Sivakumar, K.-M. Cho, and B.-T. Oh (2015). *Mater. Lett.* **138**, 272–275.
3. K. Shameli, M. B. Ahmad, W. M. Z. Wan Yunus, N. A. Ibrahim, Y. Gharayebi, and S. Sedaghat (2010). *Int. J. Nanomed.* **5**, 1067–1077.
4. K. Shameli, M. B. Ahmad, W. M. Z. Wan Yunus, et al. (2010). *Int. J. Nanomed.* **5**, 875–887.
5. F. M. Reicha, A. Sarhan, M. I. Abdel-Hamid, and I. M. El-Sherbiny (2012). *Carbohydr. Polym.* **89**, 236–244. https://doi.org/10.1016/j.carbpol.2012.03.002.
6. K. Shameli, M. B. Ahmad, M. Zargar, W. M. Z. Wan Yunus, A. Rustaiyan, and N. A. Ibrahim (2010). *Int. J. Nanomed.* **6**, 581–590.
7. K. Shameli, M. B. Ahmad, W. M. Z. Wan Yunus, and N. A. Ibrahim (2010). *Int. J. Nanomed.* **5**, 743–751.
8. K. Shameli, M. B. Ahmad, M. Zargar, W. M. Z. Wan Yunus, and N. A. Ibrahim (2011). *Int. J. Nanomed.* **6**, 331–341.
9. K. Shameli, M. B. Ahmad, S. D. Jazayeri, et al. (2012). *Int. J. Mol. Sci.* **13**, 6639–6650.
10. M. Ramayal and M. S. Subapriya (2012). *Int. J. Pharm. Med. Biol. Sci.* **1**, (1), 54–61.
11. S. P. Chandran, M. Chaudhary, R. Pasricha, A. Ahmad, and M. Sastry (2006). *Biotechnol. Prog.* **22**, 577–583. https://doi.org/10.1021/bp0501423.
12. A. Bankar, B. Joshi, A. R. Kumar, and S. Zinjarde (2010). *Colloids Surf. A Physicochem. Eng. Aspects* **368**, 58–63.
13. P. Sivakumar, C. Nethradevi, and S. Renganathan (2012). *Asian J. Pharm. Clin. Res.* **5**, (3), 97–101.
14. S. P. Dubey, M. Lahtinen, and E. Sillanpaa (2010). *Process Biochem.* **45**, 1065–1071.
15. K. Sivaranjani and M. Meenakshisundaram (2013). *Int. Res. J. Pharm.* **4**, (1), 225–229.
16. D. Jain, H. K. Daima, S. Kachhwaha, and S. L. Kothari (2009). *Digest J. Nanomater. Biostruct.* **4**, 557–563.
17. B. Ankamwar, C. Damle, A. Ahmad, and M. Sastry (2005). *J. Nanosci. Nanotechnol.* **5**, (10), 1665–1671.
18. R. Kirubha and G. Alagumuthu (2013). *Asian J. Pharm. Clin. Res.* **6**, (4), 60–64.
19. N. Ahmad, K. Shree, M. Srivastava, and R. Dutta (2014). *Int. J. Pharmacol. Pharm. Sci.* **1**, 28–31.
20. M. N. Nadagouda and R. S. Varma (2008). *Green Chem.* **10**, 859–862.
21. R. Kirubha and G. Alagumuthu (2014). *IJPRBS* **3**, (5), 287–297.
22. J. Palanivelu, M. M. Kunjumon, A. Suresh, A. Nair, and C. Ramalingam (2015). *J. Pharm. Sci. Res.* **7**, (9), 690–695.
23. N. S. Paul and R. P. Yadav (2015). *J. Biomed. Pharm. Sci.* **5**, (45), 26–28.
24. A. Lalitha, R. Subbaiya, and P. Ponmurugan (2013). *Int. J. Curr. Microbiol. Appl. Sci.* **2**, (6), 228–235.

25. Karthik K, Dhuskodi S. *Structural and optical properties of microwave-assisted CdO-NiO nanocomposite*. in AIP Conf. Proc. 2016; 1731,050021.

26. A. Sahai and N. Goswami (2014). *Physica E.* **58**, 130–137.

27. S. Akhlaghi, M. Kalalee, S. Mazinani, et al. (2012). *Thermochim Acta.* **527**, 91–98.

28. T. R. Tatarchuk, N. D. Paliychuk, M. Bououdina, B. Al-Najar, M. Pacia, W. Macyk, and A. Shyichuk (2018). *J. Alloys Compd.* **731**, 1256–1266.

29. B. Rajesh Babu and T. Tatarchuk (2018). *Mater. Chem. Phys.* **207**, 534–541.

30. P. Logeswari, S. Silambarasan, and J. Abraham (2015). *J. Saudi Chem. Soc.* **19**, 311.

31. M. Forough and K. Farhadi (2010). *Turkish J. Eng. Environ. Sci.* **34**, 281.

32. S. Gurunathan, K. Kalishwaralal, R. Vaidyanathan, D. Venkataraman, and S. R. Pandian (2009). *Colloids Surf. B Biointerfaces.* **74**, 328–335.

33. S. Gaikwad, A. Ingle, A. Gade, M. Rai, A. Falanga, N. Incoronato, et al. (2013). *Int J. Nanomed.* **8**, 4303–4314.

34. V. Revathi and K. Karthik (2018). *J. Emerg. Technol. Innov. Res.* **5**, (3), 1035–1039.

35. J. Mores, J. Elechiguerra, A. Camacho, H. Katherine, B. Juan, R. Jose Tapia, and J. Mifuel (2005). *Nanotechnology* **16**, 2346–2353.

36. J. Kim, S. Sung, S. Moon, J. Choi, J. Kim, and D. Lee (2008). *J. Microbiol. Biotechnol.* **18**, 1482–1484.

37. K. Karthik, S. Dhanuskodi, C. Gopinath, S. Prabukumar, and S. Sivaramakrishnan (2017). *J. Mater. Sci. Mater. Electron.* **28**, 11420–11429.